Exciton-Exciton Interactions in AlAs/GaAs Coupled Quantum Wire Arrays

T. Mélin and F. Laruelle

Laboratoire de Microstructures et de Microélectronique, Centre National de la Recherche Scientifique, 196 Avenue Henri Ravera, BP 107, 92225 Bagneux Cedex, France

(Received 10 July 1998)

We perform optical spectroscopy on quasi-1D excitons appearing in low disorder AlAs/GaAs lateral superlattices (LSLs) achieved by organized growth on vicinal substrates. Exciton-exciton couplings are measured by bringing optical levels into resonance in tilted LSLs. In a regime where the large LSL periodicity preserves the 2D Rydberg (E_B), we report unexpected splittings as high as $0.37E_B$ (6 times the 2D values). This enhancement of Coulomb interaction is analyzed in terms of valence-band mixing and 1D periodic confinement. [S0031-9007(98)07611-X]

PACS numbers: 71.35.Cc, 73.20.Dx, 78.55.Cr, 78.66.Fd

Exemplar manifestation of exalted Coulomb interactions in semiconductor nanostructures comes from the enhancement of excitonic binding energies with reduced dimensionalities. This picture, which is now well established for ground optical states in two and one dimensions [1], breaks down in the case of excited optical transitions, where the Coulomb interaction leads to exciton-exciton couplings, small and weakly dependent on the dimensionality in 3D and 2D [2,3]. Such couplings are probed experimentally by bringing excitonic transitions into resonance with an external perturbation. In bulk GaAs, $2s$ heavy hole (HH) and $1s$ light hole (LH) excitons exhibit an anticrossing of 0.3 meV (0.05 times the exciton binding energy E_B) under uniaxial pressure [2], which goes up to 0.7 meV ($0.07E_B$) in a 16 nm GaAs quantum well (QW) under electric field [3]. The role played by exciton-exciton interactions in lower dimensionalities is crucial to understand optical spectra of quantum wires (QWRs) and quantum dots and is still open. In the absence of theoretical predictions, it has been indeed difficult to address this topic from previous experimental data [4,5], since QWRs are very sensitive to size fluctuations disorder.

We measure and analyze here Coulomb interactions between quasi-1D excitons appearing in absorption spectra of extremely low disorder AlAs/GaAs lateral superlattices (LSLs) (which are coupled QWRs). The LSL 1D optical transitions are first identified by comparing the optical absorption and its linear and circular polarization properties with a band-to-band calculation. Exciton-exciton couplings are then probed by bringing excitonic states into resonance by using the LSL tilt effect (Fig. 1) [6]. We observe an unexpected splitting of 4.4 meV or $0.37E_B$ (6 times the 2D values) between HH and LH $1s$ excitonic states at the edge and at the center of the Brillouin minizone defined by the LSL periodicity. It is unambiguously evidenced by the exchange of oscillator strength and of hole angular momentum. This huge excitonic interaction is shown to originate in the LSL reduced dimensionality and in the valence band mixing.

LSLs are achieved by ordered molecular beam epitaxy (MBE) growth on (001) GaAs vicinal substrates misoriented by 0.5° towards (110) to define a monomolecular step array with a period $L_x = 32$ nm after the growth of a GaAs buffer layer in the step-flow mode [7]. We use a new LSL growth scheme to minimize step disorder [8]. Each LSL layer nominally consists in a monolayer fraction $m \simeq 0.1$ of AlAs followed by a monolayer fraction $n \simeq 0.9$ of GaAs to exactly cover the terraces ($m + n = 1$). The previous sequence is repeated $N = 36$ times and embedded between two AlAs barriers for vertical confinement along the growth axis z. This realizes a 10-nm-thick $Al_{0.1}Ga_{0.9}As/AlAs$ quantum well with a lateral confinement of peak-to-peak amplitude up to 50 meV stemming from the partial ordering of Al atoms at the step edges during the growth [4,9,10]. The LSL tilt comes from the imperfect surface coverage $m + n = 1 + \varepsilon$, which creates a $2\pi N\varepsilon$ phase shift between the first and the last LSL monolayers (Fig. 1a). A continuous set of ε values is obtained due to flux gradients in the MBE chamber (Fig. 1b). In tilted LSLs, the 1D potential seen

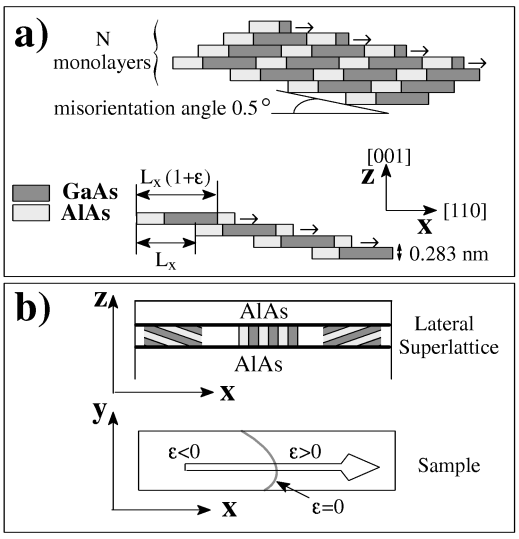

FIG. 1. (a) Schematic ideal cross section of a LSL with the definition of L_x and ε. (b) Schematic side and top views of the sample to illustrate the change of ε. The open arrow depicts the scan of the laser spot on the sample.

 0031-9007/98/81(20)/4460(4)$15.00

by electrons of the ground subbands confined along z (E_1, HH_1, or LH_1) follows a sinusoidal law of period L_x with an effective amplitude depending on the tilt parameter $N\varepsilon$ [6] as

$$V_{1D}^{N\varepsilon}(x) = \left[\frac{1}{1 - N^2\varepsilon^2}\,\frac{\sin(\pi N\varepsilon)}{\pi N\varepsilon}\right] V_{1D}\cos\left(\frac{2\pi x}{L_x}\right).$$

The amplitude is obviously maximum for $N\varepsilon = 0$ (V_{1D}) and decreases to zero for large LSL tilt.

We perform photoluminescence (PL) spectroscopy at 1.8 K in superfluid helium with an experimental setup described elsewhere [4]. By scanning the 40 μm laser spot along the wafer, we probe the optical properties for various tilt values. The PL excitation (PLE) linear polarization ratio (LPR) is defined as LPR $= (I_\perp - I_\parallel)/(I_\perp + I_\parallel)$, where $I_\perp$ and $I_\parallel$ are the PL intensities for the exciting laser light polarized, respectively, perpendicular and parallel to the wires. Each optical transition associated with a 1D miniband exhibits a specific LPR determined by the HH-LH valence band mixing [4,5,11]. The PLE circular polarization ratio (CPR) is defined as CPR $= (I_+ - I_-)/(I_+ + I_-)$, where I_+ (I_-) denotes the PL intensity polarized along σ^+ (σ^-) for a σ^+ exciting laser light. A positive (negative) CPR reveals a HH (LH) dominant optical transition in QW or QWR [5,12,13].

Figure 2a displays the PL, PLE spectra with the PLE LPR and CPR for a nontilted LSL. The low sample disorder is evidenced through the small PL linewidth and PLE Stokes shift for $N\varepsilon = 0$ (respectively, 3.0 and 5.8 meV), which slightly increase compared to $|N\varepsilon| \gg 1$ (respectively, 2.0 and 4.0 meV). These data are compared to the calculated band-to-band absorption spectrum shown in Fig. 2b together with valence and conduction minibands in Fig. 2c [14]. For $N\varepsilon = 0$, the periodic confinement forms minibands and opens minigaps at the critical points of the band structure in $(k_x, k_y) = (p\pi/L_x, 0)$ for $p = 1, 2, \ldots$ in the valence band (VB) and conduction band (CB). Major optical transitions take place at the miniband onsets either at the center or at the edge of the mini-Brillouin zone where the joint density of states is singular [16]. Using a rigid 2D Rydberg, we make a direct *quantitative* comparison between the calculated band-to-band absorption (used to identify and label the optical transitions) and the PLE experimental data. This is justified since the LSL periodicity ($L_x = 32$ nm) is larger than the exciton Bohr radius ($a_B = 9$ nm) as can be seen from recent calculations [1,17]. PLE transitions are labeled e_m-hh_n or e_m-lh_n, where m and n denote the mth and nth lateral minibands of the first CB subband E_1 and two first VB subbands HH_1 or LH_1. They are identified as follows.

e_1-hh_1 is the ground E_1HH_1 transition redshifted compared to $V_{1D} = 0$. Its negative LPR comes from the coupling between the $(k_x = 0, k_y = 0)$ heavy-hole state with the $(\pm 2\pi/L_x, 0)$ HH-LH mixed states.

e_1-hh_3 occurs between the onsets of the third lateral miniband in VB and the first in CB. It is forbidden in 2D since it involves a $(\pm 2\pi/L_x, 0)$ VB state and a $(0, 0)$ CB state. The necessary overlap to make this transition optically active is brought by the zone-folding effect. Calculated and experimental relative oscillator strengths of e_1-hh_1 and e_1-hh_3 are in good agreement. The characteristic e_1-hh_3 positive LPR (+37% in PLE) is well reproduced by the calculated one (+27%).

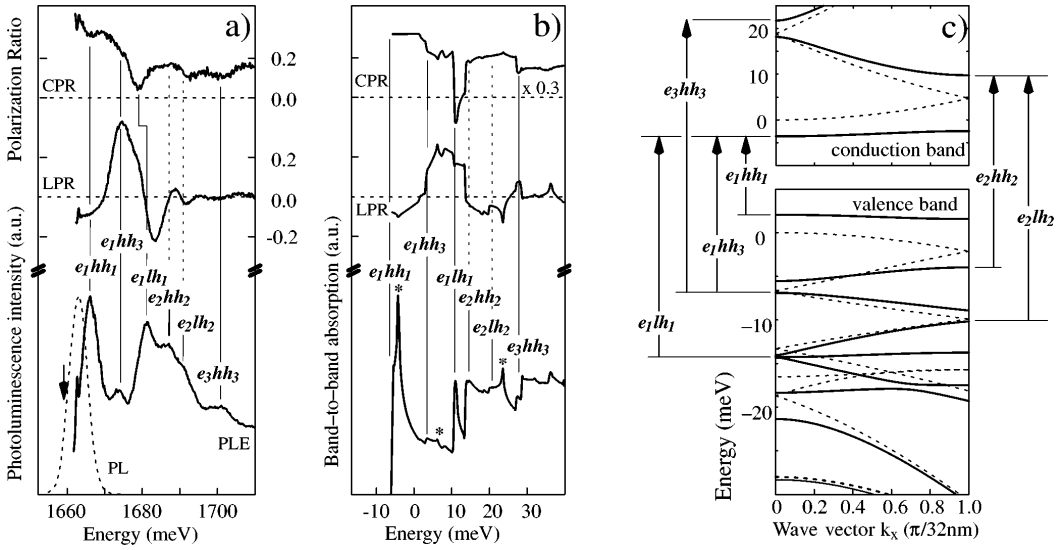

FIG. 2. (a) Measured PL, PLE, LPR, and CPR spectra. The arrow shows the monitored PL window used for PLE. The PLE CPR is obtained with the PL being detected with σ^+ polarization. (b) Calculated band-to-band absorption, LPR and CPR spectra. Stars denote saddle-point singularities. Transitions correlated with CPR and LPR features are indicated by solid vertical lines, uncorrelated ones by dotted lines. (c) $k_y = 0$ dispersion curves of tilted ($V_{1D} = 0$, dotted lines) and untilted (solid lines) LSLs. Anticrossings between HH and LH dispersion curves occur systematically for $N\varepsilon = 0$ because of valence-band mixing and lateral couplings. Transitions are labeled according to the text.

e_1-lh_1 is the ground light-hole transition, redshifted as e_1-hh_1. Its light-hole character is revealed by its measured and calculated CPR dip.

e_2-hh_2 involves the onsets of the second lateral minibands above the first minigaps opened in $(\pm\pi/L_x, 0)$ in CB and VB. By essence it is blueshifted with respect to the case $V_{1D} = 0$. Since e_1 and hh_1 minibands are not significantly dispersed along k_x, a measure of the total minigaps in CB and VB is given by the energy difference between e_2-hh_2 and e_1-hh_1. As expected, the measured value (20.3 meV) is close to the amplitude used in the calculation ($V_{1D} = 19$ meV).

e_2-lh_2 is the similar LH transition. As a result of the electronlike curvature of the LH_1 dispersion curve, the energy difference between e_2-lh_2 and e_1-lh_1 is no longer the total valence and conduction minigaps. Experimental (9.8 meV) and calculated (9.4 meV) values are indeed reduced and in very good agreement.

e_3-hh_3 is the transition between zone-folded states at the onsets of the third HH and conduction lateral minibands. The LH dominant character (CPR dip in PLE and in the calculations) of the $(2\pi/L_x, 0)$ states involved here is due to valence-band mixing.

We now focus on the e_2-hh_2 and e_1-lh_1 transitions. As the tilt is increased, the system becomes 2D-like and e_2-hh_2 lies below e_1-lh_1 since the summed kinetic energy in π/L_x in VB (2.2 meV) and CB (4.7 meV) is less than the HH_1-LH_1 splitting (16.5 meV) (Fig. 2c). These transitions are thus expected to come into resonance for intermediate tilt. A marked anticrossing occurs in Fig. 3 where the PLE and CPR spectra are displayed for various $N\varepsilon$ values, restricted to $N\varepsilon < 0$ values (the same holds for $N\varepsilon > 0$). First e_2-hh_2 and e_1-lh_1 exchange their oscillator strengths ($-0.87 \leq N\varepsilon \leq -0.75$) while the negative dip associated to E_1LH_1 in CPR ($|N\varepsilon| \gg 1$) is gradually blurred. A small replica of this LH signature develops on the low energy peak of the doublet for $|N\varepsilon| \leq 0.8$ which shows the exchange of hole angular momentum.

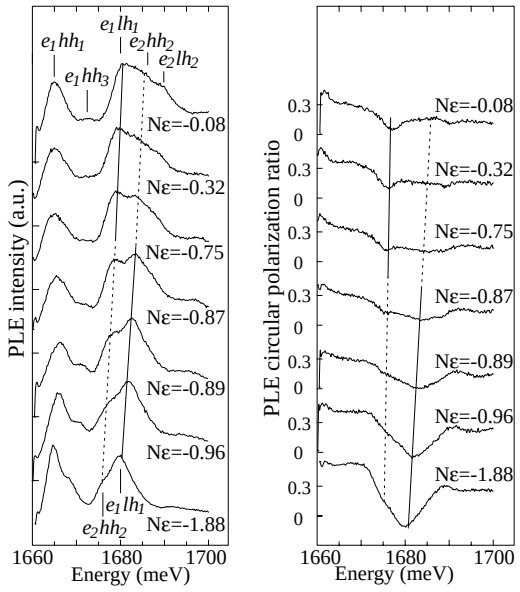

FIG. 3. LSL PLE spectra (left) and CPR spectra (right) for different $N\varepsilon$ values. Solid (dotted) lines are guides to the eye and refer to e_1-lh_1 (e_2-hh_2) transitions.

To quantify this, the tilt dependence of the main PLE lines is compared to the band-to-band calculations in Fig. 4. The energy of E_1HH_1, extrapolated for $V_{1D} = 0$, is taken as a reference thus correcting all energies for the LSL thickness dependence except the HH-LH splitting decreasing with $N\varepsilon$ (thin solid lines in Fig. 4). The e_1-hh_1 redshift and the e_1-hh_3 line are well fitted for $N\varepsilon \neq 0$. This demonstrates the relevance of our treatment of tilt effects and also that the exciton binding energy remains 2D in coupled QWRs [17]. By tilting the LSL, the calculated e_2-hh_2 and e_1-lh_1 become degenerate for $|N\varepsilon| = 0.6$, in good agreement with the experimental data which shows a maximum mixing for $|N\varepsilon| \simeq 0.8$. We recalculate the e_2-hh_2 and e_1-lh_1 energies as a function of tilt using an empirical, tilt independent, coupling of 2.2 ± 0.2 meV in a two-level model (thick solid line in Fig. 4). This nicely fits the experimental data for $|N\varepsilon| \leq 1$. Couplings are still efficient even for $N\varepsilon = 0$ and explain why e_2-hh_2 and e_1-lh_1 are not correlated to PLE LPR and CPR extrema since they are mixed and of opposite signs in the calculation (vertical dotted lines in Figs. 2a and 2b).

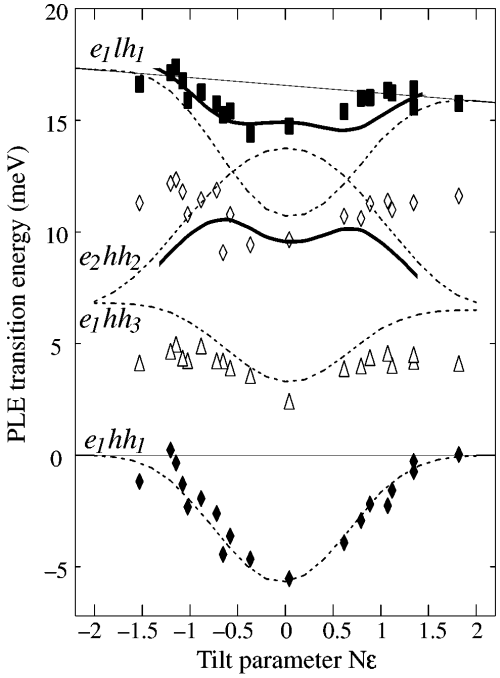

FIG. 4. Symbols: energies of experimental PLE lines corrected for the LSL thickness dependence (see text) as a function of the tilt parameter. Thin solid lines: reference 2D energies of E_1HH_1 and E_1LH_1. Dotted lines: calculated energies of e_1-hh_1, e_1-hh_3, e_2-hh_2, and e_1-lh_1 as a function of $N\varepsilon$. Thick solid lines: recalculated e_2-hh_2 and e_1-lh_1 energies with a two-level model (see text).

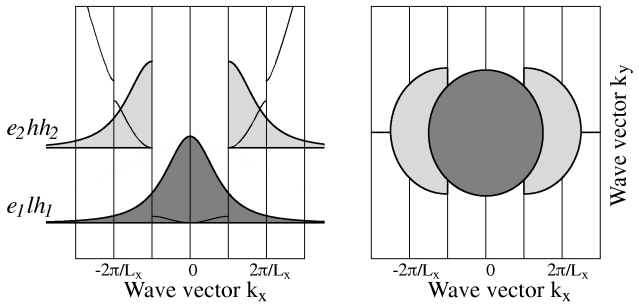

FIG. 5. Left: zone-center (dark gray) and zone-edge (light gray) schematic exciton wave functions used to describe e_1-lh_1 and e_2-hh_2. The conduction-band dispersion law is added for sake of clarity. Right: schematic representation of the e_1-lh_1 and e_2-hh_2 excitons in the (k_x, k_y) plane.

We calculate this excitonic splitting in the formalism of Ref. [18] which describes quantitatively the excitonic interaction due to VB mixing in 2D [3] by computing the c-matrix element of the Luttinger Hamiltonian between pure HH and LH excitons. Here the pure LH wave function is defined by a $1s$ 2D state at the zone center (it spreads over the 1st, 2nd, ... Brillouin minizones) while the HH zone-edge exciton is defined *outside* the first lateral minizone (it spreads over the 2nd, 3rd, ... Brillouin minizones) (Fig. 5). Because $\pi/L_x \simeq 1/a_B$, the two HH and LH excitons fairly overlap around $(\pi/L_x, 0)$ though they are separated in k space. Since the c term of the Luttinger Hamiltonian is proportional to k^2 along k_x, the calculated splitting (2.0 meV) using a 2D band structure, i.e., $V_{1D} = 0$, is already boosted compared to Ref. [3]. The higher experimental splitting (4.4 meV) is assigned to the 1D periodic confinement which should explain the remaining 2.4 meV. Although the e_2-hh_2 and e_1-lh_1 excitons are separated by π/L_x, they are efficiently coupled by the lateral potential (which couples states differing by $\Delta k_x = \pm 2\pi/L_x$) since they spread in k space over $1/a_B$. This contributes to enhance the global interaction. Its detailed calculation will require a larger basis of excited excitonic states in the presence of VB mixing. This falls beyond the scope of this paper.

In conclusion, we have shown that in LSLs where the 2D ground state exciton binding energy is preserved due to lateral tunnel coupling, interaction between excited excitonic states is strongly enhanced compared to 2D and 3D cases. This observation has been possible thanks to the very low sample disorder and to the tunability of the LSL confinement by the tilt effect. This finding opens the question of exciton-exciton interaction in quantum dots where the quantum confinement is even stronger. Modifications of absorption spectra brought by this effect should be carefully considered while designing semiconductor nanostructures for optoelectronic applications.

We thank F. Lelarge, F. Petit, P. Denk, C. Tanguy, R. Planel, and B. Etienne for stimulating discussions. IFCPAR Grant No. 1514-1 and DRET are gratefully acknowledged for financial support.

[1] See, e.g., F. Rossi, G. Goldoni, and E. Molinari, Phys. Rev. Lett. **78**, 3527 (1997), and references therein.
[2] C. Jagannath and E. S. Koteles, Solid State Commun. **58**, 417 (1986).
[3] L. Viña *et al.*, Phys. Rev. Lett. **58**, 832 (1987).
[4] J. Bloch *et al.*, Europhys. Lett. **28**, 501 (1994).
[5] F. Vouilloz *et al.*, Phys. Rev. Lett. **78**, 1580 (1997).
[6] T. Mélin and F. Laruelle, Phys. Rev. Lett. **76**, 4219 (1996); T. Mélin and F. Laruelle, Surf. Sci. **361/362**, 762 (1996).
[7] F. Lelarge *et al.*, Europhys. Lett. **39**, 97 (1997).
[8] Ga and Al are supplied in a pulsed mode as usual for LSL growth. But the As_4 flux is continuously delivered and is minimized to ensure the surface stoichiometry. This is found to lower considerably the LSL disorder. This scheme slightly reduces the LSL amplitude (by 20%) compared to our best results [9] because of a lower migration length.
[9] F. Laruelle, in *Low Dimensional Structures Prepared by Epitaxial Growth or Regrowth on Patterned Substrates*, edited by K. Eberl, P. M. Petroff, and P. Demeester, NATO ASI Ser. E (Kluwer Academic Publishers, Dordrecht, The Netherlands, 1995), p. 111.
[10] F. Lelarge *et al.*, Europhys. Lett. **40**, 213 (1997).
[11] U. Bockelmann and G. Bastard, Europhys. Lett. **15**, 215 (1991); Phys. Rev. B **45**, 1688 (1992).
[12] C. Weisbuch, R. C. Miller, R. Dingle, A. C. Gossard, and W. Wiegman, Solid State Commun. **37**, 219 (1981).
[13] A. Twardowsky and C. Hermann, Phys. Rev. B **35**, 8144 (1987).
[14] We use the envelope function approach of Ref. [11] to calculate the band-to-band absorption from the Fermi golden rule. A $0.078m_0$ electron mass accounts for the mean LSL Al content ($\simeq$0.1). The Luttinger Hamiltonian parameters are those of Ref. [15]. V_{1D} is the only adjustable parameter which is set to 19 meV to compute the in-plane band structure with lateral couplings up to the fifth order. Tilt effects are included according to Ref. [6]. To get the theoretical CPR we assume a complete hole spin relaxation and multiply the CPR by 0.3 because of a partial electron spin depolarization [13].
[15] B. V. Shanabrook *et al.*, Phys. Rev. B **39**, 3411 (1989).
[16] We consider only critical points of the band structure for which dispersion along k_x and k_y have the same sign and discard saddle-point excitons which have a much lower oscillator strength (stars in Fig. 2b).
[17] H. Ando *et al.*, Phys. Rev. B **55**, 2429 (1997).
[18] G. Bastard, J. A. Brum, and R. Ferreira, *Electronic States in Semiconductor Heterostructures*, Solid State Physics Vol. 44, edited by H. Ehrenreich and D. Turnbull (Academic Press, New York, 1991), p. 229.